MODELLING MAGNETO-OPTICAL RESONANCES IN ATOMIC RUBIDIUM AT D_1 EXCITATION IN EXTREMELY THIN CELLS WHILE MAINTAINING A SELF-CONSISTENT SET OF THEORETICAL PARAMETERS

L. KALVANS*, M. AUZINSH, R. FERBER, F. GAHBAUER and A. JARMOLA

Laser Centre, The University of Latvia, 19 Rainis Boulevard, LV-1586 Riga, Latvia
**E-mail: linards.kalvans@lu.lv*

A. PAPOYAN and D. SARKISYAN

Institute for Physical Research, NAS of Armenia, Ashtarak-0203, Armenia

Nonlinear magneto-optical resonances of alkali atoms have been studied both experimentally and theoretically with high accuracy in ordinary vapor cells. By using an extremely thin cell (ETC), Doppler broadening is reduced so that all hyperfine transitions can be resolved. To study the magneto-optical resonances, an ETC containing a natural mixture of atomic rubidium was placed at the center of a three-axis Helmholtz coil system, which canceled the ambient magnetic field. The magnetic field was controlled and scanned from −60 G to +60 G along the axis that was perpendicular to both the polarization direction and propagation direction of the laser radiation. The theoretical model was based on the optical Bloch equations; careful comparison of experimental and theoretical results allowed us to find the right model to account for transit relaxation, laser power density, and Doppler broadening, the theoretical results presented here were obtained by a self-consistent set of parameters.

Keywords: Magneto-optical resonances.

1. Introduction

The introduction of atomic vapor cells of size of few hundred nanometers has provided a number of new research and application opportunities in magnetometry and optoelectronics.[1,2] Such cells are called extremely thin cells (ETCs). In the ETCs sub-Doppler spectroscopy becomes possible when the exciting laser light is propagating normally with respect to the cell windows. In such a setup only the atoms flying nearly parallel to the windows are able to interact with the exciting laser, as the rest of the atoms suf-

fer from frequent collisions with the cell walls, which prevents them from reaching the excited state and fluorescing. In this paper the above properties of ETCs are exploited for research of magneto-optical resonances, which occur in the fluorescence plots versus magnetic field at zero field values. The resonance is expected to be bright[3] when the quantum number of the total angular momentum of the ground state hyperfine level F_g is less than the corresponding quantum number for the excited state F_e. Otherwise ($F_g \geq F_e$), the resonance is expected to be dark.[4,5] The resonances are formed as a result of the fact that at zero magnetic field the magnetic sublevels of the ground state form a quantum superposition state, which is coupled to the exciting laser field (bright resonance) or not coupled (dark resonance). When the magnetic field is applied, the superposition state is destroyed, which leads to changes in the fluorescence signal. Despite the simple principles of the theoretical description, the theoretical calculations have produced a number of controversial results. One of the reasons for these calculations have produced controversies might be lack of ability to resolve distinct hyperfine transitions under the Doppler profile. This problem could be overcome by using ETCs. The first results of this approach[6] produced some unexpected results – resonances observed bright in an ordinary vapor cell appeared to be dark in an ETC. Our goal for this study was to clarify the situation by recording experimental data of magneto-optical resonances and applying a theoretical model proven to be successful in cm-sized cells.[7,8] In order to do so we had to find the best adjustment for the parameters in the model to fit the specific conditions of ETC.

The D_1 line of alkali metals consists of four hyperfine components. The hyperfine level splittings and relative strengths of transistions are shown in Fig. 1. The FWHM of Doppler profile at room temperature (in an

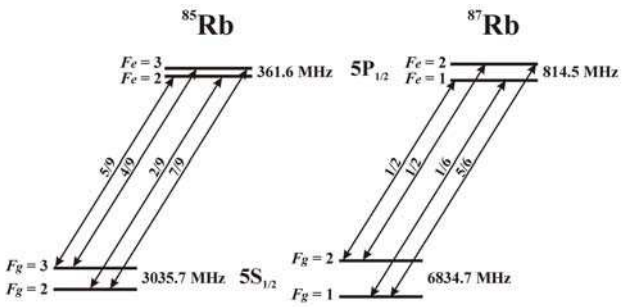

Fig. 1. Hyperfine level structure and transitions of the D_1 line of rubidium. The fractions on the arrows indicate the relative transition strengths.[9,10]

ordinary vapor cell) is about 500 MHz, which fully covers the excited state splitting for the ^{85}Rb isotope and partially for ^{87}Rb. However, in the ETC the Doppler profile is reduced, as mostly the atoms flying nearly parallel to the cell windows determine the fluorescence signal, and, thus, the hyperfine transitions become completely resolved.

2. Experimental Setup

The ETC was produced at the Institute of Physical Research in Ashtarak, Armenia, while the experiments described here were performed in Riga. The principle of the ETC is described in Refs. 1, 11. The cell windows, are two perfectly polished wafers made from YAG crystal that are glued in such a way that the distance between windows changes from 50 nm to roughly 2 μm, thus allowing the experimenter to choose the desired windows separation Rubidium is stored in a side arm bonded to the main cell. Appropriate vapor pressure was maintained by heating the side arm to 150^{o}C and windows to 200^{o}C in a two-chambered oven, thus preventing a formation of metal coating on the cell windows. A Toptica DL 100 external-cavity, single-mode diode laser with a wavelength of 794.3 nm and a typical linewidth of a few megahertz was used for the experiment. The laser wavelength was monitored by a High Finesse WS-7 wavemeter without using any active stabilization. To maintain the necessary linear polarization and control the power density, the laser beam was passed through a Glan-Thomson polarizer. The beam profile was checked by a Thorlabs BP 104-VIS beam profiler. A typical beam covered an area of 0.15 cm^2 (although it was different for a number of experiments), and the power density was altered between 10 mW/cm^2 and 2000 mW/cm^2.

In order to apply the magnetic field, three pairs of Helmholtz coils were used, two of which compensated the ambient laboratory magnetic field, while the third generated the scan magnetic field in the same direction along which the fluorescence was detected. The excitation, observation and magnetic field geometry can be seen in Fig. 2. In most cases the magnetic field was scanned from negative to positive values at fixed laser frequency, but for some transitions the double-scan technique[12] was used – the laser was scanned slowly across the transition while rapidly changing the magnetic field. In a typical scan the laser frequency would change by 2–5 MHz while the magnetic field was changed over the whole range (up to $\pm$60 G).

The fluorescence that emerged via the side walls of the ETC was detected by means of a Thorlabs FDS-100 photodiode without singling out any particular polarization direction. Results were recorded for both ru-

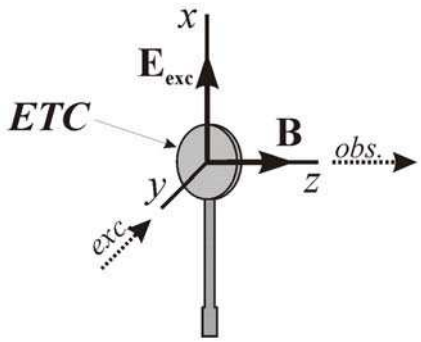

Fig. 2. Experimental geometry. The relative orientation of the laser beam (exc), laser light polarization ($\mathbf{E}_{exc}$), magnetic field ($\mathbf{B}$), observation direction (obs), and ETC walls are shown.

bidium isotopes and for all four hyperfine transitions of each isotope. To tune laser to a particular hyperfine transition, peaks in the fluorescence versus laser frequency were detected at zero magnetic field. For each transition and power density several scans were made and averaged. If there was significant deviation in results of some scans they were excluded from the averaged results.

3. Theoretical Model

A theoretical model had been developed previously in order to describe bright and dark resonances in ordinary vapor cells[7,8] where a detailed description can be found. Here we present just the final equations with brief comments. The equations are based on optical Bloch equations, which describe the time evolution of the semi-classical atomic density matrix ρ:[13]

$$i\hbar\frac{\partial\rho}{\partial t} = \left[\hat{H},\rho\right] + i\hbar\hat{R}\rho. \tag{1}$$

The Hamiltonian $\hat{H}$ is considered to consist of the unperturbed atomic Hamiltonian – H_0, an operator H_B, which describes the atomic interaction with the external magnetic field, and the dipole interaction operator $\hat{V}$. The relaxation operator $\hat{R}$ includes the spontaneous decay rate Γ_N and transit relaxation rate γ. Applying the rotating wave approximation and considering the Doppler shits due to the classical motion of atoms, stochastic differential equations are obtained. The latter are further simplified by the decorrelation approach.[14] Finally the optical coherences are eliminated

and we obtain rate equations for Zeeman coherences:

$$\frac{\partial \rho_{g_i g_j}}{\partial t} = \left(\Gamma_{p,g_i e_m} + \Gamma^*_{p,e_k g_j}\right) \sum_{e_k,e_m} \left(d_1^{g_i e_k}\right)^* d_1^{e_m g_j} \rho_{e_k e_m}$$
$$- \sum_{e_k,g_m} \left[\Gamma^*_{p,e_k g_j} \left(d_1^{g_i e_k}\right)^* d_1^{e_k g_m} \rho_{g_m g_j} + \Gamma_{p,g_i e_k} \left(d_1^{g_m e_k}\right)^* d_1^{e_k g_j} \rho_{g_i g_m}\right]$$
$$-i\omega_{g_i g_j} \rho_{g_i g_j} + \sum_{e_i,e_j} \Gamma^{e_i e_j}_{g_i g_j} \rho_{e_i e_j} - \gamma \rho_{g_i g_j} + \lambda\delta\left(g_i, g_j\right) \quad (2)$$

and

$$\frac{\partial \rho_{e_i e_j}}{\partial t} = \left(\Gamma^*_{p,e_i g_m} + \Gamma_{p,g_k e_j}\right) \sum_{g_k,g_m} d_1^{e_i g_k} \left(d_1^{g_m e_j}\right)^* \rho_{g_k g_m}$$
$$- \sum_{g_k,e_m} \left[\Gamma_{p,g_k e_j} d_1^{e_i g_k} \left(d_1^{g_k e_m}\right)^* \rho_{e_m e_j} + \Gamma^*_{p,e_i g_k} d_1^{e_m g_k} \left(d_1^{g_k e_j}\right)^* \rho_{e_i e_m}\right]$$
$$-i\omega_{e_i e_j} \rho_{e_i e_j} - \Gamma \rho_{e_i e_j}. \quad (3)$$

These equations are pretty easy to understand qualitatively as each term describes some logical subprocess in atom-laser interaction. The density matrix elements for ground and excited state Zeeman coherences are denoted by $\rho_{g_i g_j}$ and $\rho_{e_i e_j}$. In equation 2 the first term describes induced transfers that repopulate the ground state, $\Gamma_{p g_i e_m}$ and Γ^*_{p,ekg_i} stand for the coupling induced by the laser between ground and excited states and are dependent on the Rabi frequency Ω_R, the natural linewidth Γ_N, the laser linewidth, the laser detuning from the frequency of a particular transition, and the central velocity of the atomic velocity group while performing averaging over the Doppler profile; $d_1^{e_i g_j}$ is the dipole transition matrix element between the ground state i and the excited state j. The second term (whole sum in the square brackets) describes the population loss in the ground state due to laser absorption processes. The third term describes the splitting of the Zeeman sublevels in the magnetic field and can be calculated by means of the Breit-Rabi formula.[15,16] The fourth term stands for the repopulation of the ground state via the spontaneous decay of the excited state, the fifth – relaxation of the ground state due to transit relaxation (or collisions with with the cell walls in the case of ETC). And finally, the sixth term is there for the repopulation of the ground state due to depolarized atoms arriving in the interaction region (either flying in or being depolarized after collision with the cell wall).

In the equation 3 the first term describes how population of the excited state increases due to light absorption while the second denotes the population lost via induced transitions. The third term describes level splitting

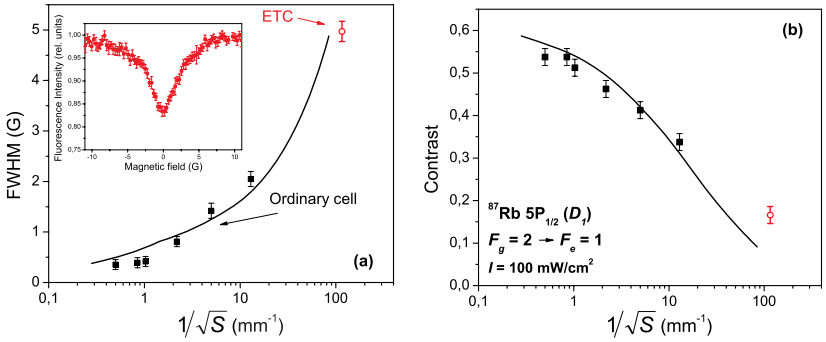

Fig. 3. Resonance (a) width and (b) contrast as a function of the inverse size of the interaction region with the beam: the square root of the cross-sectional area of the beam in the case of the ordinary cell[8] and the characteristic length before collision in case of the ETC. Filled squares experiment in an ordinary cell; open circles: experiment in an ETC; solid curve: theory. The inset in (a) shows a typical dark resonance in the ETC. Data are for the $F_g = 2 \rightarrow F_e = 1$ transition of ^{87}Rb at a laser power density of 100 mW/cm^2.

in the magnetic field and the fourth, the relaxation of the ground state via spontaneous emission (rate – Γ_N) and transit/collisions (rate – γ).

The equations 2 and 3 are considered for stationary conditions $\partial\rho/\partial t = 0$, where they form a system of linear equations, which can be solved numerically to obtain the density matrices for the ground and excited states. The assumption of stationary conditions means that the characteristic relaxation and coupling times of atomic system are much lower than the interaction times at the same conditions (magnetic field values), which holds true for our experimental conditions. Once the density matrices are known, the fluorescence signal can be calculated to a constant factor for particular observation geometry as follows:

$$I_f(\tilde{\mathbf{e}}) = \tilde{I}_0 \sum_{g_i,e_i,e_j} d^{(ob)*}_{g_i e_j} d^{(ob)}_{g_i e_i} \rho_{e_i e_j}, \tag{4}$$

where $\tilde{I}_0$ is a constant of proportionality.

One of the parameters that determined the width and contrast of the resonances in the theoretical description of ordinary vapor cells was the transit relaxation rate γ, which is the rate at which atoms fly out of the region of interaction with the laser radiation. This transit relaxation rate thus is related to the laser beam diameter. The solid squares in Fig. 3 mark the dependence of the resonance width and contrast on the inverse square root of the cross-sectional area S of the beam, which is related to the inverse

of the laser beam diameter in the ordinary cell. In the ETC, resonances are significantly broader than in ordinary cells, and their contrast is much smaller. The question arises: are the resonance width and contrast in the ETC still controlled by a transit relaxation rate γ, and, if so, what is the length corresponding to this transit relaxation rate? In our experiments the laser beam diameter was much larger than the ETC wall separation; thus, the characteristic length in the ETC should be related to the wall separation rather than to the laser beam diameter. However, a Voigt profile fit to the fluorescence peaks in an LIF excitation spectrum of the ETC revealed that the Doppler width in the ETC is approximately 60 MHz (FWHM) when the wall separation L is equal to the wavelength λ of the laser radiation. The Doppler width corresponding to that temperature in an ordinary cell would be about ten times greater. One could therefore say that a typical atom that fluoresces and travels at the average thermal speed flies on a trajectory that makes an angle with respect to the ETC wall such that the flight path between the walls is about ten times the wall separation. Indeed, the abscissa of the open circles in Fig. 3, which correspond to the resonance width and contrast in the ETC, have been chosen to correspond to a length dimension that is about ten times the wall separation, and the circles lie rather close to the extrapolation of the theoretical model developed for ordinary cells. Strictly speaking, it is not correct to extend the theoretical calculation with the parameter values chosen for ordinary cells into the regime of the ETC. However, Fig. 3 suggested that a single theoretical approach might be able to describe qualitatively the width and contrast of nonlinear magneto-optical resonances in alkali vapors over several orders of magnitude of a single dimension, which is related to a transit relaxation rate γ. Hence, we formulated the hypothesis that the shapes of nonlinear magneto-optical resonances in an ETC can be described by the same model that describes these signals in ordinary cells when the particular characteristics of the ETC are reflected in appropriately chosen values of the model parameters.

4. Analysis of Results

According to the rules stated in section 1 one would expect to observe three dark and one bright resonance for each isotope. The experimental and theoretical results in Fig. 4 and Fig. 5 clearly indicate the three dark resonances for transitions $F_g = 3 \rightarrow F_e = 2$, $F_g = 3 \rightarrow F_e = 3$, and $F_g = 2 \rightarrow F_e = 2$ for ^{85}Rb, and $F_g = 2 \rightarrow F_e = 1$, $F_g = 2 \rightarrow F_e = 2$, and $F_g = 1 \rightarrow F_e = 1$ for ^{87}Rb. On the other hand the small peaks of

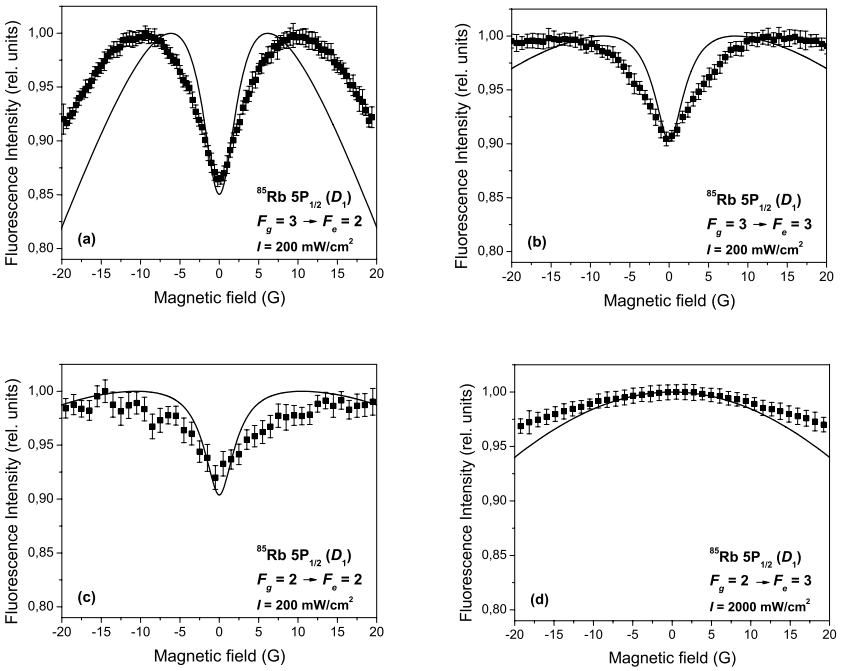

Fig. 4. Fluorescence intensity versus magnetic field for ^{85}Rb at D_1 excitation. Filled squares, experiment; solid line, theory. The excited state, total angular momentum of the ground F_g and excited states F_e of the transition, and laser power density I are given in each panel. Wall separation $L = \lambda$, the wavelength of the light.

the bright resonance observed in the ordinary cell[7,8] have disappeared both from the theoretical and experimental results. This might be explained by the increased transit/collision relaxation rate γ in the ETC conditions, which is the main parameter determining the shape of the resonance – the smaller is its value the more narrow is the peak of the resonance. In the case of the ETC it has most likely become so wide that it is not resolvable under the wide shape of the decreasing fluorescence as a result of the magnetic field shifting the Zeeman sublevels out of resonance with the laser field.

A lot of effort was applied to fit the experimental and theoretical results as the theoretical model does not allow to predict exact Rabi frequencies for particular laser power density. In addition, the most effective value of the transit/collision rate γ had to be established. Of no less importance was the estimation of the residual Doppler profile in the ETC and the value of the background signal present in the experimental data. In order

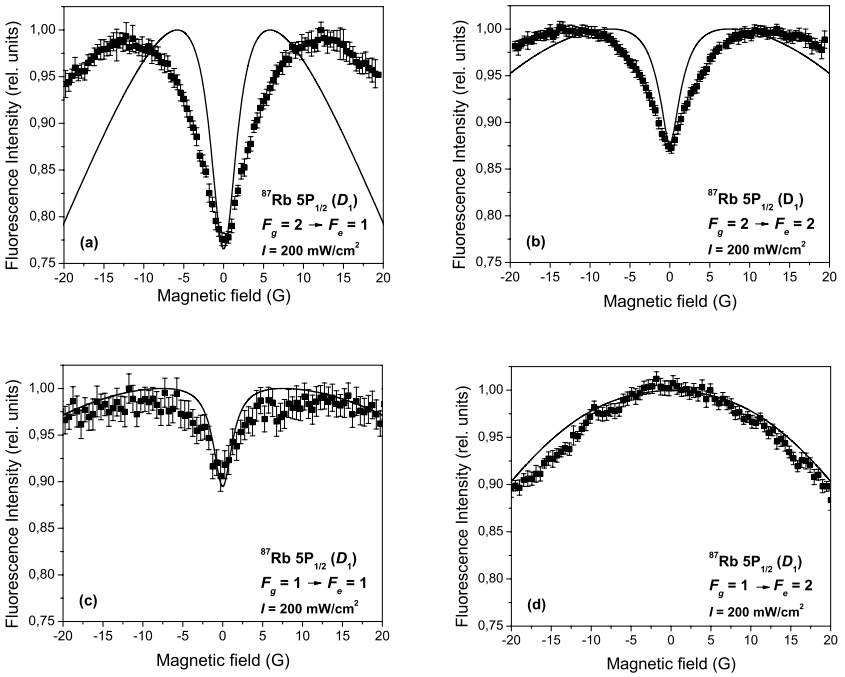

Fig. 5. Fluorescence intensity versus magnetic field for ^{87}Rb at D_1 excitation. Filled squares, experiment; solid line, theory. The excited state, total angular momentum of the ground F_g and excited states F_e of the transition and laser power density I are given in each panel. Wall separation $L = \lambda$, the wavelength of the light.

to obtain the best values for these parameters, a number of theoretical calculations were run with various parameter sets, and the one that gave the best correspondence for all the hyperfine transitions and both isotopes was chosen for the final results. It is worth noting that our aim was to use the same parameters for all transitions while for each particular transition better consistency could be achieved with slightly different parameters. The parameters chosen for the final results were as follows: the laser power density was related to the Rabi frequency as $I = \Omega_R^2$, the transit/collision rate γ=1.44 MHz, the FWHM for the residual Doppler profile was 60 MHz, and the background signal in the experimental results was 50%, while the spectral linewidth of laser was assumed to be 10 MHz. Once established, the same parameters were used for all calculations.

Figure 6 shows the transition $F_g = 1 \rightarrow F_e = 1$ for ^{87}Rb at various laser power densities. The filled squares represent experimental results while the

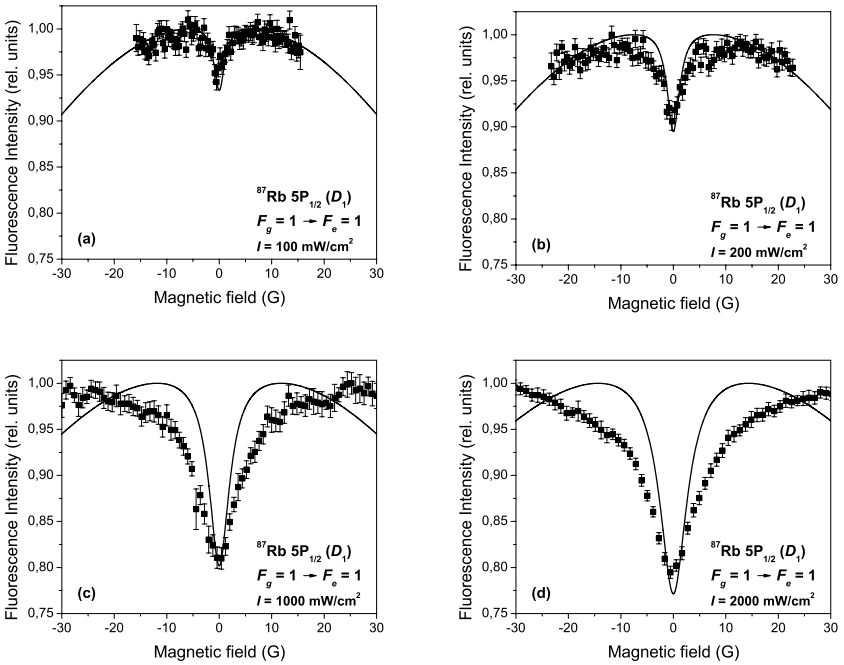

Fig. 6. Resonance signals for ^{87}Rb at the $F_g = 1 \rightarrow F_e = 1$ transition for different laser power densities I. Filled squares, experiment; solid line, theory. $L = \lambda$.

solid line denotes the results of theoretical calculations. Similar to the case of ordinary vapor cells, discrepancies between theory and experiment arise when the laser power density (and, hence, the Rabi frequency) is increased. The discrepancies mostly affect the shape of the resonances, especially at larger field values, while the contrast is still described very well even at high laser power densities (Fig. 7). The reason of this most likely is the exponential transit/collision relaxation mechanism assumed in the model is not valid at higher Rabi frequencies, and some nonlinear mechanism should be considered.

As was seen in the case of the ordinary cell (see Fig. 6 in Ref. 8) the resonances are sensitive to detuning, in the case of an ETC one would expect a much larger sensitivity as the Doppler profile is significantly reduced. Indeed, as can bee seen in Fig. 8, there is a rapid drop in the resonance contrast when the detuning the laser frequency changes by just a few tens of megahertz. In fact, the contrast drop in an ETC at 20 MHz detuning roughly equals the contrast drop in an ordinary cell when laser

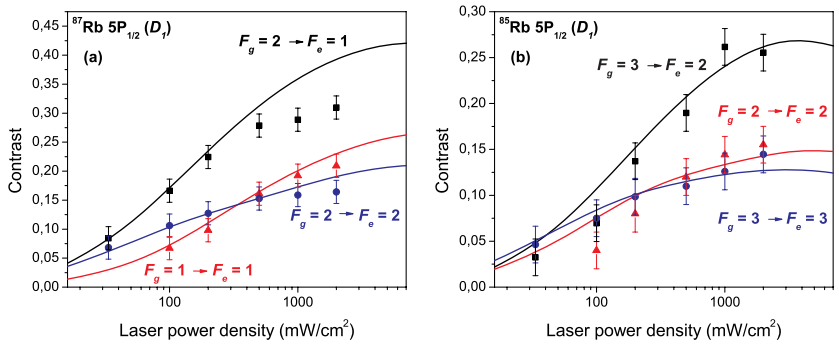

Fig. 7. Resonance contrast as a function of laser power density for (a) ^{87}Rb and (b) ^{85}Rb dark resonances. Markers, experiment; solid line, theory. $L = \lambda$.

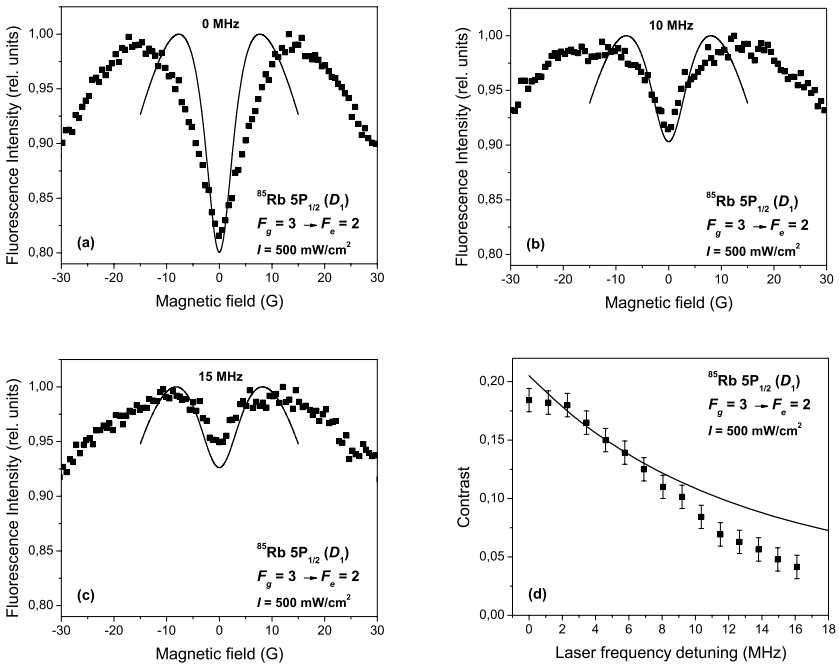

Fig. 8. Resonance signals for ^{87}Rb at the $F_g = 1 \rightarrow F_e = 1$ transition for different laser power densities I. Filled squares, experiment; solid line, theory. $L = \lambda$.

is detuned by 300 MHz. These results also are in agreement with results of the dark resonance formation in an ETC in a Λ-system with two lasers (^{85}Rb $5S_{1/2}$,$F_g = 2 \rightarrow 5P_{3/2} \rightarrow 5S_{1/2}$,$F_g = 3$).[17,18] Namely, as the coupling laser was detuned from the resonance with an atomic transition, a strong increase of the resonance width of the electromagnetically induced transparency and a worsening of the contrast were recorded. In ordinary cm-size cells, effectively the opposite behavior would be observable.

Due to the wedge form of the ETC it was possible to obtain resonance signals for various wall separation distances. The separation could be changed and controlled simply by changing the position of incident beam on the cell and observing the intensity of transmitted light, which obeyed the Fabri-Perot rules and produced maximal signal when wall separation equals an integer times half the wavelength. We have measured resonances for L equal to $\lambda/2$, $3\lambda/4$, λ, and $3\lambda/2$, and the results are shown in Fig. 9. In order to model these results we assumed that transit/relaxation time γ^{-1} and the residual Doppler profile are linearly proportional to the cell thickness, decreasing if the separation is decreased and vice versa. As can be seen in Fig. 9, this does a pretty good job in describing the contrast changes, although it fails to predict the width dynamics of the resonances. In this case we did not explore the dependence on wall separation in more detail, but some nonlinear effects might be responsible for the severe change in resonance shape while changing wall separation.

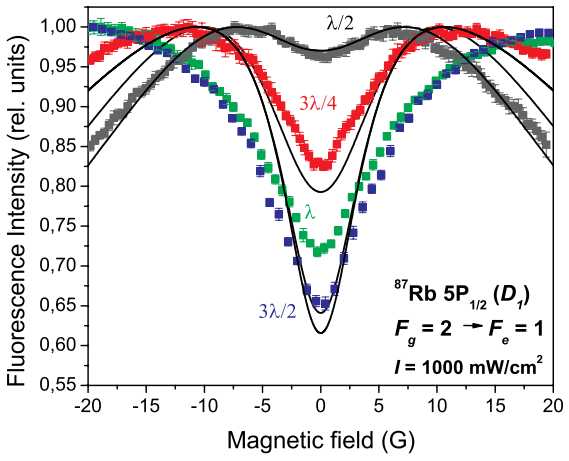

Fig. 9. Resonance signals for ^{87}Rb at the $F_g = 1 \rightarrow F_e = 1$ transition for different laser power densities I. Filled squares, experiment; solid line, theory. $L = \lambda$.

In general the agreement between the experimental data and calculations was satisfactory over a wide range of different experimental conditions and for four distinct hyperfine transitions in each of two isotopes, though it was not nearly as good as in case of an ordinary cell.[8] Several reasons can be named that could be responsible for the discrepancies in the case of ETC. First of all, as a result of the sensitivity of the resonance shapes to the laser detuning (Fig. 8), in the case of the ETC, small inevitable drifts in the laser frequency could cause significant changes in measurements, whereas in the case of ordinary cell, such drifts would make very little difference. Secondly, since the signals are sensitive to the cell thickness (Fig. 9) and since the cell thickness is a nonlinear function of position and is changing rapidly, the actual laser beam (0.4 mm in diameter) covered a region of varying cell thickness.

5. Conclusions

Nonlinear magneto-optical resonances have been measured for all hyperfine transitions of the D_1 line of ^{85}Rb and ^{87}Rb in an ETC under a wide variety of experimental conditions, which included different laser power densities, laser detunings, and ETC thicknesses. As expected, six dark resonances have been observed on hyperfine transitions with $F_g \geq F_e$. The expected bright resonances ($F_g < F_e$) where not observed, in agreement with the theoretical model. The theoretical model was based on the optical Bloch equations and was essentially the same as the one used to describe the resonances in ordinary cells, although some parameters where changed to adapt the model to the case of the ETC. These parameters included the non-coherent transit/collision relaxation rate γ, which was increased considerably, and the residual Doppler profile. which was decreased, to meet the conditions atoms face in the thin space between the cell windows. The last parameter to change was the conversion factor between Rabi frequency and laser power density. With all these parameters changed, satisfactory agreement between theory and experiment was achieved using the same parameter set for all hyperfine transitions in both isotopes. Overall, the resonances in the ETC are much broader and have lower contrast when compared to resonances in ordinary cells. The observations are strongly supported by the results of theoretical model and our understanding of physical processes present in the described conditions.

The theory does a pretty good job at describing the resonances at low power densities and the overall dynamics of the dark resonance contrasts while changing the laser power density. Problems arise when describing the

shape of the resonance at higher laser power densities, especially when predicting the shape of the resonance "wings", i.e., the part of the signal at higher magnetic field values after the maximum in the fluorescence signal has been reached. It is worth pointing out the high sensitivity of the resonances to laser detuning from the exact hyperfine transition frequency, which is very well described by the theoretical model. Another interesting result concerns changes in resonance shape with changing wall separation. However, this result still lacks a full theoretical understanding and should be subject to further investigations.

Acknowledgments

The Riga group would like to thank Maris Tamanis for assistance with the experiments and Christina Andreeva for useful discussions and to acknowledge support from the Latvian National Research Programme in Material Sciences Grant No. 1-23/50 and the Latvian Science Council Grant No. LZP 09.1196. The work in Ashtarak was supported in part by the INTAS South-Caucasus Grant 06-1000017-9001. L. K. acknowledges support from the ESF project Nr. 2009/0138/1DP/1.1.2.1.2./09/IPIA/VIAA/004, and F. G. acknowledges support from the ESF project Nr. 2009/0223/1DP/1.1.1.2.0./09/APIA/VIAA/008.

References

1. D. Sarkisyan and A. Papoyan, *Optical processes in micro- and nanometric thin cells containing atomic vapor* (Nova Science Publishers, 2009), vol. 263 of *Horizons in World Physics*, chap. 3, pp. 85124.
2. A. Sargsyan, G. Hakhumyan, A. Papoyan, D. Sarkisyan, A. Atvars, and M. Auzinsh, Applied Physics Letters **93**, 021119 (2008).
3. Y. Dancheva, G. Alzetta, S. Cartalava, M. Taslakov, and C. Andreeva, Optics Communications **178**, 103 (2000).
4. G. Alzetta, A. Gozzini, L. Moi, and G. Orriols, Il Nuovo Cimento B **36**, 5 (1976).
5. R.W. Schmieder, A. Lurio,W. Happer, and A. Khadjavi, Physical Review A **2**, 1216 (1970).
6. C. Andreeva, A. Atvars, M. Auzinsh, K.Bluss, S. Cartaleva, L. Petrov, and D. Slavov, Physical Review A **76**, 063804 (2007).
7. M. Auzinsh, R. Ferber, F. Gahbauer, A. Jarmola and L. Kalvans, Physical Review A **78**, 013417 (2008), ISSN 10941622.
8. M. Auzinsh, R. Ferber, F. Gahbauer, A. Jarmola and L. Kalvans, Physical Review A **79**, 053404 (2009), ISSN 10941622.
9. D. A. Steck, *Rubidium 85 D line data* (2009), (revision 2.1.2, 12 August 2009), URL http://steck.us/alkalidata.

10. D. A. Steck, *Rubidium 87 D line data* (2009), (revision 2.1.2, 12 August 2009), URL http://steck.us/alkalidata.
11. D. Sarkisyan, D. Bloch, A. Papoyan, and M. Ducloy, Optics Communications **200**, 201 (2001).
12. C. Andreeva, S. Cartaleva, Y. Dancheva, V. Biancalana, A. Burchianti, C. Marinelli, E. Mariotti, L. Moi, and K. Nasyrov, Physical Review A **66**, 012502 (2002), ISSN 10941622.
13. S. Stenholm, *Foundations of Laser Spectroscopy* (Dover Publications, Inc., Mineole, New York, 2005).
14. N. G. van Kampen, Physics Reports **24**, 171 (1976).
15. G. Breit and I. I. Rabi, Physical Review **38**, 2082 (1931), ISSN 15366065.
16. E. B. Aleksandrov, M. Chaika and G. I. Khvostenko *Interefernce of Atomic States* (Springer Verlag, Berlin, 1993).
17. A. Sargsyan, D. Sarksiyan and A. Papoyan, Physical Review A **73**, 033803 (2006), ISSN 10941622.
18. Y. Pashayan-Leroy, C. Leroy, A. Sargsyan, A. Papoyan and D. Sarkisyan, J. Opt. Soc. Am. B **24**, 1829 (2007).